

Dark particle mass effects on neutron star properties from a short-range correlated hadronic model

M. Dutra,^{*} C. H. Lenzi, and O. Lourenço

Departamento de Física, Instituto Tecnológico de Aeronáutica, DCTA, 12228-900, São José dos Campos, SP, Brazil

21 November 2022

ABSTRACT

In this work we study a relativistic mean-field (RMF) hadronic model, with nucleonic short-range correlations (SRC) included, coupled to dark matter (DM) through the Higgs boson. We study different parametrizations of this model by running the dark particle Fermi momentum, and its mass in the range of $50 \text{ GeV} \leq M_\chi \leq 500 \text{ GeV}$, compatible with experimental spin-independent scattering cross-sections. By using this RMF-SRC-DM model, we calculate some neutron star quantities, namely, mass-radius profiles, dimensionless tidal deformabilities, and crustal properties. Our findings show that is possible to construct RMF-SRC-DM parametrizations in agreement with constraints provided by LIGO and Virgo collaboration (LVC) on the GW170817 event, and recent observational data from the NICER mission. Furthermore, we show that the increase of M_χ favors the model to attain data from LVC regarding the tidal deformabilities. Higher values of M_χ also induce a reduction of the neutron star crust (mass and thickness), and cause a decrease of the crustal fraction of the moment of inertia (I_{crust}/I). Nevertheless, we show that some RMF-SRC-DM parametrizations still exhibit $I_{\text{crust}}/I > 7\%$, a condition that explains the glitch activity in rotation-powered pulsars such as the Vela one. Therefore, dark matter content can also be used for describing such a phenomenon.

Key words: Neutron Stars – Equation of States – Dark Matter

1 INTRODUCTION

A compact star (CS) is a highly dense astrophysical object composed by hadrons, leptons, and/or quark matter (Lattimer & Prakash 2007; Lattimer 2012; Menezes 2021; Stone 2021; Annala et al. 2020). Therefore, a deep understanding of strong and weak interactions is extremely important in order to correctly describe this system. For the theoretical formulation of the former at the hadronic level, many phenomenological models with a huge amount of parametrizations have been used over the years, such as the Skyrme (Dutra et al. 2012; Lourenço et al. 2020) and relativistic mean-field (RMF) models (Dutra et al. 2014a, 2016a,b, 2014b). With the same aim, quark-meson coupling models, in which nucleons are explicitly formed by interacting quarks, are also frequently adopted for nuclear and stellar matter description (Stone et al. 2022; Guichon et al. 2018; Guichon 1988; Frederico et al. 1989; Lourenço et al. 2021). The CS environment can be used to test the interactions allowed by these different models. In that sense, the stellar matter is seen as a natural laboratory, not possible to be reproduced in terrestrial experiments (at least so far), in which the extreme condition of high density is possible to be attained.

Recently, many observational data were obtained and used as constraints to select the more suitable models and parametrizations, and consequently the related physics, capable of better explaining different CSs global properties. As an example of these

updated data, we address the reader to the multimessenger astronomy era, started from the detection of gravitational waves originated by the collision of black holes (Abbott et al. 2016b,c,a) and by the CSs merging (Abbott et al. 2017; Cowperthwaite et al. 2017; Abbott et al. 2020). From the latter (GW170817 event), limits on the tidal deformabilities were also inferred (Abbott et al. 2018). The x-ray telescope based at the International Space Station, and responsible for NASA’s Neutron star Interior Composition Explorer (NICER) mission (Gendreau et al. 2016), also provided valuable information on the mass-radius relation of CSs, determined from measurements of the pulsars PSR J0030+0451 (Miller et al. 2019; Riley et al. 2019) and PSR J0740+6620 (Miller et al. 2021; Riley et al. 2021). Furthermore, accurate mass measurements recently led to $M = 2.08^{+0.07}_{-0.07} M_\odot$ for massive CSs, according to Fonseca et al. (2021). In summary, there is a lot of recent astrophysical information that can be used to test the limits of hadronic phenomenological models and their different versions.

The attempt of satisfying all aforementioned observational constraints, and other ones, led to the inclusion of other degrees of freedom beyond baryons, mesons, quarks, and gluons in the formulation of refined hadronic and quark models for the dense matter. An example is the inclusion of dark matter (DM) in the equations of state furnished as input for the construction of stellar matter. Indications of the existence of this kind of matter were given in the 70’s by Vera Cooper Rubin, who verified that the rotational velocity of stars around the center of spiral galaxies (v_r) does not obey gravitation theory, which predicts $v(r) \approx \sqrt{M_g/r}$ (r is the distance of the star from the galaxy center, and M_g is the galaxy mass). In (Rubin et al.

^{*} E-mail: marianad@ita.br

1978), rotation curves of a sample of 10 high-luminosity spiral galaxies were analyzed, with the approximate flat format verified for all of them, indicating that $v(r)$ is roughly constant. From the previous expression for $v(r)$, one observes that such a result is only possible if M_g increases proportionally to r , i.e., the mass of the galaxies should be higher than the observed visible matter (they would contain massive halos). This non detected mass, named dark matter, was earlier suggested by astronomer Fritz Zwicky (Zwicky 1933, 2009). His measurements and calculations for the Coma cluster led him to increase the mass of each galaxy of the cluster by two orders of magnitude, indicating that it is not composed only of luminous matter. Similar results were also found by Jan Hendrik Oort (Oort 1932), who studied the gravitational force perpendicular to the galactic plane. Despite the research on this subject presents many evidences of the existence of DM, its exact nature is not yet completely understood. There are different types of possible DM candidates, such as weakly interacting massive particles (WIMP), sterile neutrinos, axinos, gravitinos, axions, Q-balls, WIMPzillas, supersymmetric, and mirror matter (Feng 2010; Kusenko & Rosenberg 2013). Recent studies have been developed in which dark particle candidates are coupled to hadrons in order to describe CSs properties, see for instance Das et al. (2022a,b); Panotopoulos & Lopes (2017); Das et al. (2019); Quddus et al. (2020); Das et al. (2020, 2021a,b,c,d); Kumar et al. (2022).

CSs are suitable environments for DM binding because they are extremely massive systems (around $2M_\odot \approx 10^{30}$ kg) and, therefore, gravitational interaction is very intense. Other type of interactions between DM and observable matter are also possible, since some upper limits are verified. In particular, in Lourenço et al. (2022a,b) the lightest neutralino with mass of $M_\chi = 200$ GeV was used as dark particle coupled through the Higgs boson to nucleons presenting short-range correlations (SRC) (Hen et al. 2014; CLAS Collaboration 2018, 2019; Schmidt et al. 2020; Hen et al. 2017; Duer et al. 2019; Li et al. 2008; Cai & Li 2016; Guo et al. 2021; Cai & Li 2022; Souza et al. 2020). Such correlations are experimentally verified in electron-induced quasielastic proton knockout reactions, in which nucleons correlate in pairs with high relative momentum. The effect of this phenomenology is observed in the single-nucleon momentum distribution, $n(k)$, in finite nuclei and nuclear matter, where a high momentum tail of the form k^{-4} takes place. This new structure for $n(k)$ changes all kinetic terms of the hadronic model and, consequently, all related thermodynamics even at the zero temperature regime, used to construct the equations of state for the stellar matter description. In this work, we use this particular model coupled to dark matter (RMF-SRC-DM model) to calculate CSs global properties, namely, mass-radius diagrams, dimensionless tidal deformabilities related to the GW170817 event, and also some specific properties of the crust such as mass, thickness, and the fraction of the moment of inertia. Unlike in Lourenço et al. (2022a,b) in which the dark particle mass was kept fixed in $M_\chi = 200$ GeV, we now let this quantity to run inside the range of $50 \text{ GeV} \leq M_\chi \leq 500 \text{ GeV}$. Our results point out the possibility of generating RMF-SRC-DM parametrizations, with different values of M_χ , capable of reproducing observational data from the GW170817 event, and the recent findings of the NICER mission. Concerning the crustal properties, we also show that the increase of M_χ reduces both, the CS crust region and also a crustal fraction of the moment of inertia. Even with the latter effect, we show that this quantity can attain a value greater than 7%. As this particular constraint is used to explain the glitches observed in pulsars such as the Vela one, it can not be disregarded the possibility of this phenomenon being induced by dark matter.

This paper is divided as follows: In Sec. 2 we present the formal-

ism of coupling between DM and the hadronic model with short-range correlations included. The Lagrangian density and the main thermodynamical equations of state are also shown in this section. Sec. 3 contains our results. More specifically, in Sec. 3.1 mass-radius profiles and dimensionless tidal deformabilities are tested against the variation in both, M_χ and the dark particle Fermi momentum. Crustal properties are calculated in Sec. 3.2. Finally, we close the manuscript with a summary and concluding remarks in Sec. 4.

2 DARK MATTER-HADRONIC MODEL WITH SHORT-RANGE CORRELATIONS

The model used in this work considers nucleons (protons/neutrons), with short-range correlations included, interacting with each other through mesons exchange and with a certain dark matter content. The hadronic part of the system is described by the following Lagrangian density

$$\begin{aligned} \mathcal{L}_{\text{HAD}} = & \bar{\psi}(i\gamma^\mu \partial_\mu - M_{\text{nuc}})\psi + g_\sigma \sigma \bar{\psi}\psi - g_\omega \bar{\psi}\gamma^\mu \omega_\mu \psi \\ & - \frac{g_\rho}{2} \bar{\psi}\gamma^\mu \vec{\rho}_\mu \vec{\tau}\psi + \frac{1}{2}(\partial^\mu \sigma \partial_\mu \sigma - m_\sigma^2 \sigma^2) - \frac{A}{3}\sigma^3 - \frac{B}{4}\sigma^4 \\ & - \frac{1}{4}F^{\mu\nu}F_{\mu\nu} + \frac{1}{2}m_\omega^2 \omega_\mu \omega^\mu + \frac{C}{4}(g_\omega^2 \omega_\mu \omega^\mu)^2 - \frac{1}{4}\vec{B}^{\mu\nu}\vec{B}_{\mu\nu} \\ & + \frac{1}{2}\alpha'_3 g_\omega^2 g_\rho^2 \omega_\mu \omega^\mu \vec{\rho}_\mu \vec{\rho}^\mu + \frac{1}{2}m_\rho^2 \vec{\rho}_\mu \vec{\rho}^\mu. \end{aligned} \quad (1)$$

The fields of this theory, namely, ψ , σ , ω^μ , and $\vec{\rho}_\mu$, represent the nucleon and the mediators (mesons) σ , ω , and ρ , with the respective masses given by M_{nuc} , m_σ , m_ω , and m_ρ . The coupling constants g_σ , g_ω , g_ρ , A , B , C and α'_3 control the strength of each interaction, and the tensors read $F_{\mu\nu} = \partial_\nu \omega_\mu - \partial_\mu \omega_\nu$ and $\vec{B}_{\mu\nu} = \partial_\nu \vec{\rho}_\mu - \partial_\mu \vec{\rho}_\nu$.

In order to describe the entire system with dark matter interacting with hadrons, we adopt the same Lagrangian density used in Lourenço et al. (2022a,b), namely,

$$\begin{aligned} \mathcal{L} = & \bar{\chi}(i\gamma^\mu \partial_\mu - M_\chi)\chi + \xi h \bar{\chi}\chi + \frac{1}{2}(\partial^\mu h \partial_\mu h - m_h^2 h^2) \\ & + f \frac{M_{\text{nuc}}}{v} h \bar{\psi}\psi + \mathcal{L}_{\text{HAD}}, \end{aligned} \quad (2)$$

in which the dark fermion is represented by the Dirac field χ with mass M_χ . The interaction between χ and ψ is due to the Higgs boson (scalar field h) with mass $m_h = 125$ GeV, and its strength is regulated by the constant fM_{nuc}/v , where $v = 246$ GeV is the Higgs vacuum expectation value. The constant ξ is related to the Higgs-dark particle coupling. Here we use $\xi = 0.01$ (Lourenço et al. 2022a,b), and the central value $f = 0.3$ obtained in Cline et al. (2013, 2015). According to Bhat & Paul (2020), these values ensure a spin-independent scattering cross-sections in agreement with experimental data from PandaX-II (Tan et al. 2016), LUX (Akerib et al. 2017), and DarkSide (Marini et al. 2016) collaborations for dark fermion mass in the range of $50 \text{ GeV} \leq M_\chi \leq 500 \text{ GeV}$.

The use of the mean-field approximation in this theory leads to $\sigma \rightarrow \langle \sigma \rangle \equiv \sigma$, $\omega_\mu \rightarrow \langle \omega_\mu \rangle \equiv \omega_\mu$, $\vec{\rho}_\mu \rightarrow \langle \vec{\rho}_\mu \rangle \equiv \vec{\rho}_{0(\mu)}$, and $h \rightarrow \langle h \rangle \equiv h$. This procedure is useful to determine the field equations,

namely,

$$m_\sigma^2 \sigma = g_\sigma \rho_s - A\sigma^2 - B\sigma^3 \quad (3)$$

$$m_\omega^2 \omega = g_\omega \rho - Cg_\omega (g_\omega \omega_0)^3 - \alpha'_3 g_\omega^2 g_\rho^2 \bar{\rho}_{0(3)}^2 \omega_0, \quad (4)$$

$$m_\rho^2 \bar{\rho}_{0(3)} = \frac{g_\rho}{2} \rho_3 - \alpha'_3 g_\omega^2 g_\rho^2 \bar{\rho}_{0(3)} \omega_0^2, \quad (5)$$

$$[\gamma^\mu (i\partial_\mu - g_\omega \omega_0 - g_\rho \bar{\rho}_{0(3)} \tau_3/2) - M^*] \psi = 0, \quad (6)$$

$$m_h^2 h = \xi \rho_s^{\text{DM}} + f \frac{M_{\text{nuc}}}{v} \rho_s \quad (7)$$

$$(\gamma^\mu i\partial_\mu - M_\chi^*) \chi = 0, \quad (8)$$

with $\tau_3 = 1$ (-1) for protons (neutrons). The effective nucleon and dark fermion masses are

$$M^* = M_{\text{nuc}} - g_\sigma \sigma - f \frac{M_{\text{nuc}}}{v} h \quad (9)$$

and

$$M_\chi^* = M_\chi - \xi h, \quad (10)$$

respectively, and the densities are $\rho_s = \langle \bar{\psi} \psi \rangle = \rho_{s,p} + \rho_{s,n}$, $\rho = \langle \bar{\psi} \gamma^0 \psi \rangle = \rho_p + \rho_n$, $\rho_3 = \langle \bar{\psi} \gamma^0 \tau_3 \psi \rangle = \rho_p - \rho_n = (2y_p - 1)\rho$, and $\rho_s^{\text{DM}} = \langle \bar{\chi} \chi \rangle$, with

$$\rho_s^{\text{DM}} = \frac{\gamma M_\chi^*}{2\pi^2} \int_0^{k_F^{\text{DM}}} \frac{k^2 dk}{(k^2 + M_\chi^{*2})^{1/2}}. \quad (11)$$

$\gamma = 2$ is the degeneracy factor, and the proton fraction is denoted by $y_p = \rho_p/\rho$, with nucleon densities given by $\rho_{p,n} = \gamma k_{F,p,n}^3/(6\pi^2)$. The Fermi momenta related to protons/neutrons, and the dark particle, are $k_{F,p,n}$ and k_F^{DM} , respectively.

From the Lagrangian density of the system, it is possible to determine the energy-momentum tensor ($T^{\mu\nu}$), and from this quantity we obtain energy density and pressure. In our case, Eq. 2 is used to calculate $\mathcal{E} = \langle T_{00} \rangle$ and $P = \langle T_{ii} \rangle/3$. This procedure gives rise to the following expressions,

$$\begin{aligned} \mathcal{E} = & \frac{m_\sigma^2 \sigma^2}{2} + \frac{A\sigma^3}{3} + \frac{B\sigma^4}{4} - \frac{m_\omega^2 \omega_0^2}{2} - \frac{Cg_\omega^4 \omega_0^4}{4} - \frac{m_\rho^2 \bar{\rho}_{0(3)}^2}{2} \\ & + g_\omega \omega_0 \rho + \frac{g_\rho}{2} \bar{\rho}_{0(3)} \rho_3 - \frac{1}{2} \alpha'_3 g_\omega^2 g_\rho^2 \omega_0^2 \bar{\rho}_{0(3)}^2 + \mathcal{E}_{\text{kin}}^p + \mathcal{E}_{\text{kin}}^n \\ & + \frac{m_h^2 h^2}{2} + \mathcal{E}_{\text{kin}}^{\text{DM}}, \end{aligned} \quad (12)$$

and

$$\begin{aligned} P = & -\frac{m_\sigma^2 \sigma^2}{2} - \frac{A\sigma^3}{3} - \frac{B\sigma^4}{4} + \frac{m_\omega^2 \omega_0^2}{2} + \frac{Cg_\omega^4 \omega_0^4}{4} \\ & + \frac{m_\rho^2 \bar{\rho}_{0(3)}^2}{2} + \frac{1}{2} \alpha'_3 g_\omega^2 g_\rho^2 \omega_0^2 \bar{\rho}_{0(3)}^2 + P_{\text{kin}}^p + P_{\text{kin}}^n - \frac{m_h^2 h^2}{2} \\ & + P_{\text{kin}}^{\text{DM}}. \end{aligned} \quad (13)$$

The dark particle kinetic terms are

$$\mathcal{E}_{\text{kin}}^{\text{DM}} = \frac{\gamma}{2\pi^2} \int_0^{k_F^{\text{DM}}} k^2 (k^2 + M_\chi^{*2})^{1/2} dk, \quad \text{and} \quad (14)$$

$$P_{\text{kin}}^{\text{DM}} = \frac{\gamma}{6\pi^2} \int_0^{k_F^{\text{DM}}} \frac{k^4 dk}{(k^2 + M_\chi^{*2})^{1/2}}. \quad (15)$$

Concerning the hadronic part of the RMF-DM model, the inclusion of the SRC is performed by replacing the usual step functions present in kinetic terms by the one including the high momentum tail (Cai & Li 2016; Souza et al. 2020) given by $n_{n,p}(k) = \Delta_{n,p}$ for $0 < k < k_{F,n,p}$, and $n_{n,p}(k) = C_{n,p} (k_{F,n,p}/k)^4$ for

$k_{F,n,p} < k < \phi_{n,p} k_{F,n,p}$ in which $\Delta_{n,p} = 1 - 3C_{n,p} (1 - 1/\phi_{n,p})$, $C_p = C_0 [1 - C_1 (1 - 2y_p)]$, $C_n = C_0 [1 + C_1 (1 - 2y_p)]$, $\phi_p = C_0 [1 - \phi_1 (1 - 2y_p)]$ and $\phi_n = \phi_0 [1 + \phi_1 (1 - 2y_p)]$. Here we use $C_0 = 0.161$, $C_1 = -0.25$, $\phi_0 = 2.38$ and $\phi_1 = -0.56$ (Cai & Li 2016; Souza et al. 2020). It leads to the following modified kinetic terms,

$$\begin{aligned} \mathcal{E}_{\text{kin}}^{n,p} = & \frac{\gamma \Delta_{n,p}}{2\pi^2} \int_0^{k_{F,n,p}} k^2 dk (k^2 + M^{*2})^{1/2} \\ & + \frac{\gamma C_{n,p}}{2\pi^2} \int_{k_{F,n,p}}^{\phi_{n,p} k_{F,n,p}} \frac{k_{F,n,p}^4}{k^2} dk (k^2 + M^{*2})^{1/2}, \\ P_{\text{kin}}^{n,p} = & \frac{\gamma \Delta_{n,p}}{6\pi^2} \int_0^{k_{F,n,p}} \frac{k^4 dk}{(k^2 + M^{*2})^{1/2}} \\ & + \frac{\gamma C_{n,p}}{6\pi^2} \int_{k_{F,n,p}}^{\phi_{n,p} k_{F,n,p}} \frac{k_{F,n,p}^4 dk}{(k^2 + M^{*2})^{1/2}}, \end{aligned} \quad (16)$$

and modified scalar densities

$$\begin{aligned} \rho_{s,n,p} = & \frac{\gamma M^* \Delta_{n,p}}{2\pi^2} \int_0^{k_{F,n,p}} \frac{k^2 dk}{(k^2 + M^{*2})^{1/2}} \\ & + \frac{\gamma M^* C_{n,p}}{2\pi^2} \int_{k_{F,n,p}}^{\phi_{n,p} k_{F,n,p}} \frac{k_{F,n,p}^4}{k^2} \frac{dk}{(k^2 + M^{*2})^{1/2}} \end{aligned} \quad (17)$$

for protons and neutrons.

3 RESULTS

In this section, we present the predictions of the RMF-SRC-DM model regarding neutron stars properties. Specifically for the hadronic side of the system, we focus on the parametrization discussed in Piekarewicz et al. (2014), namely, TFcmx. The authors constructed RMF parametrizations with the aim of maximizing the transition pressure (p_t) at the core-crust interface, the quantity shown to be important, for instance, for the description of the pulsar Vela glitches, since the crustal moment of inertia fraction is directly affected by p_t . Furthermore, all these studied parametrizations also provide a good description of various finite nuclei properties, according to Piekarewicz et al. (2014). Concerning the bulk properties at the saturation density (ρ_0) given by the TFcmx parametrization, we list the following ones: $\rho_0 = 0.148 \text{ fm}^{-3}$, $B_0 = -16.47 \text{ MeV}$ (binding energy), $M_0^*/M_{\text{nuc}} = 0.57$ (effective nucleon mass ratio), $K_0 = 260 \text{ MeV}$ (incompressibility), $\bar{J} \equiv S(2\rho_0/3) = 29.4 \text{ MeV}$ (symmetry energy at $2\rho_0/3$) and $L_0 = 74 \text{ MeV}$ (symmetry energy slope). It is worth mentioning that this last quantity is inside of two particular ranges, namely, $L_0 = (106 \pm 37) \text{ MeV}$, pointed out in Reed et al. (2021) to be consistent with results of neutron skin thickness measurements of ^{208}Pb (Adhikari et al. 2021), and $42 \leq L_0 \leq 117 \text{ MeV}$, obtained from the analysis of charged pions spectra (Estee et al. 2021).

We emphasize that these bulk parameters were imposed in the hadronic model used here. Since its structure contains the modifications provided by the inclusion of the SRC phenomenology, the coupling constants of the RMF-SRC model must be different from those shown in Piekarewicz et al. (2014) to keep the same bulk quantities. This is the case in our study, i.e., we use here a SRC version of the TFcmx model with the same bulk parameters of the original parametrization, namely, the aforementioned ones. It was also shown in (Lourenço et al. 2022a) that the presence of SRC favors the inclusion of DM in the system since the increase of the maximum neutron star mass caused by this phenomenology (inclusion of SRC) balances the decrease induced by DM.

With regard to the dark matter side of the RMF-SRC-DM model, we explore the variation of the dark particle mass and its effects on the neutron star properties. In [Lourenço et al. \(2022a\)](#) and [Lourenço et al. \(2022b\)](#), the lightest neutralino was used as the dark matter candidate, i.e., the mass of $M_\chi = 200$ GeV was kept fixed along all calculations. Here we relax this condition and let the dark particle mass be in the range of $50 \text{ GeV} \leq M_\chi \leq 500 \text{ GeV}$. As already pointed out in Sec. 2, such interval ([Bhat & Paul 2020](#)) produces spin-independent scattering cross-sections compatible with data provided by some experiments ([Tan et al. 2016](#); [Akerib et al. 2017](#); [Marini et al. 2016](#)).

3.1 Mass-radius diagrams and tidal deformability

In order to construct the mass-radius diagrams for the RMF-SRC-DM model presented in the previous sections, it is needed to solve the Tolman-Oppenheimer-Volkoff (TOV) equations ([Tolman 1939](#); [Oppenheimer & Volkoff 1939](#)) given by

$$\frac{dp(r)}{dr} = -\frac{[\epsilon(r) + p(r)][m(r) + 4\pi r^3 p(r)]}{r^2[1 - 2m(r)/r]}, \quad (18)$$

$$\frac{dm(r)}{dr} = 4\pi r^2 \epsilon(r). \quad (19)$$

The solution of these equations is constrained to $p(0) = p_c$ (central pressure) and $m(0) = 0$. Moreover, one has $p(R) = 0$ and $m(R) \equiv M$ at the star surface, with R defining the radius of the respective star of mass M . The description of the neutron star crust is made by parts, namely, the outer crust, modeled by the Baym-Pethick-Sutherland equation of state ([Baym et al. 1971](#)) for $6.3 \times 10^{-12} \text{ fm}^{-3} \leq \rho \leq 2.5 \times 10^{-4} \text{ fm}^{-3}$ ([Piekarewicz & Fattoyev 2019](#)); [Malik et al. \(2019\)](#), and the inner crust, for which the polytropic expression $p(\epsilon) = A + B\epsilon^{4/3}$ ([Piekarewicz & Fattoyev 2019](#); [Carriere et al. 2003](#); [Gonzalez-Boquera et al. 2018](#)) is used in the range of $2.5 \times 10^{-4} \text{ fm}^{-3} \leq \rho \leq \rho_t$. The transition density, denoted by ρ_t , is found from the thermodynamical method ([Xu et al. 2009](#); [Kubis 2004](#); [Gonzalez-Boquera et al. 2019](#)). Furthermore, we consider a system composed of protons, neutrons, leptons, and dark matter under charge neutrality and β -equilibrium. Therefore, the total energy density and pressure used as input for the TOV equations are $\epsilon = \mathcal{E} + \sum_l \epsilon_l$ and $p = P + \sum_l p_l$, with \mathcal{E} and P given in Eqs. (12) and (13), respectively, with l referring to the leptons (muons, with $m_\mu = 105.7$ MeV, and massless electrons). We emphasize that in our approach, the contribution of DM is distributed in the core of the star, since for the outer shell (crust region) we assume the aforementioned construction (piecewise equation of state) in which only ordinary matter is taken into account.

In Fig. 1 we display the mass-radius diagrams generated by the RMF-SRC-DM model for three different values of the dark mass particle, namely, $M_\chi = 50$ GeV, 200 GeV and 500 GeV, and for its Fermi momentum given by $k_F^{\text{DM}} = 0.02$ GeV, $k_F^{\text{DM}} = 0.03$ GeV and $k_F^{\text{DM}} = 0.04$ GeV. For the sake of comparison, we also provide the curve related to the RMF-SRC model, i.e., without dark matter content in the system. This particular case is constructed by taking $k_F^{\text{DM}} = 0$. Rigorously, the term proportional to h^2 would still nonvanishing in Eqs. (12) and (13). However, it was shown in [Lourenço et al. \(2022a\)](#) that this particular term is negligible in comparison to the other ones. Therefore, the pure hadronic system is recovered by making $k_F^{\text{DM}} = 0$ in the equations of the model. From Fig. 1, it is clear that the inclusion of dark matter content, by taking nonvanishing values of k_F^{DM} , reduces the neutron star mass as previously mentioned. Furthermore, it is also verified that the increase of M_χ also favors this reduction. This is a feature in agreement with other studies performed

in which the dark particle mass is allowed to run, see, for instance, [Guha & Sen \(2021\)](#); [Sen & Guha \(2021\)](#); [Quddus et al. \(2020\)](#). Notice that the neutron stars radii are also highly affected by the change of M_χ . In particular, R decreases as M_χ increases and this variation is larger for higher values of k_F^{DM} .

We also depict in Fig. 1 the limiting contours related to recent observational data obtained (i) from NASA's Neutron star Interior Composition Explorer (NICER) mission, regarding measurements of pulsars PSR J0030+0451 ([Miller et al. 2019](#); [Riley et al. 2019](#)) and PSR J0740+6620 ([Miller et al. 2021](#); [Riley et al. 2021](#)), determined in 2019 and 2021, respectively, (ii) from the LIGO and Virgo Collaboration (LVC) concerning the detection of gravitational waves caused by the coalescence of a binary neutron star system, the so called GW170817 event ([Abbott et al. 2017, 2018](#)), and (iii) from a new measurement provided on the maximum neutron star mass ([Fonseca et al. 2021](#)) (horizontal dashed lines). As one can observe, it is completely possible to generate RMF-SRC-DM parametrizations, by varying k_F^{DM} and/or M_χ , in agreement with all these constraints, i.e. a certain DM content can be used to predict mass-radius diagrams simultaneously consistent with observations.

For another view of the impact of the neutralino mass on the stellar matter, we show in Fig. 2 the profiles related to stars of $1.4M_\odot$ and $1.8M_\odot$. From this figure, it is observed that the central pressure increases for higher values of M_χ , with the variation being more significant for the more massive star. Moreover, notice that the pressure change is more concentrate in the inner region of the star, in agreement with results found in [Bhat & Paul \(2020\)](#). A more detailed investigation on the size of the DM inside the star can be easily performed by adopting the two-fluid approach, in which profiles of each component can be obtained separately and, consequently, precise information regarding DM halos or DM concentrated in the CS core can be extracted. In a recent study performed in [Sagun et al. \(2022\)](#); [Giangrandi et al. \(2022\)](#), for instance, the authors shown that accumulated DM inside the star favor the compatibility with the GW170817 data.

In order to obtain the dimensionless tidal deformability, defined as $\Lambda = 2k_2/(3C^5)$, with $C = M/R$,

$$\begin{aligned} k_2 &= \frac{8C^5}{5}(1-2C)^2[2+2C(y_R-1)-y_R] \\ &\times \left\{ 2C[6-3y_R+3C(5y_R-8)] \right. \\ &+ 4C^3[13-11y_R+C(3y_R-2)+2C^2(1+y_R)] \\ &\left. + 3(1-2C)^2[2-y_R+2C(y_R-1)]\ln(1-2C) \right\}^{-1}, \quad (20) \end{aligned}$$

and $y_R = y(R)$, we proceed to determine the function $y(r)$ through the solution of the differential equation given by

$$r \frac{dy}{dr} + y^2 + yF(r) + r^2 Q(r) = 0, \quad (21)$$

solved along with the TOV equations. The quantities $F(r)$ and $Q(r)$ read

$$\begin{aligned} F(r) &= \frac{1-4\pi r^2[\epsilon(r)-p(r)]}{g(r)}, \quad (22) \\ Q(r) &= \frac{4\pi}{g(r)} \left[5\epsilon(r) + 9p(r) + \frac{\epsilon(r)+p(r)}{v_s^2(r)} - \frac{6}{4\pi r^2} \right] \\ &- 4 \left[\frac{m(r)+4\pi r^3 p(r)}{r^2 g(r)} \right]^2, \quad (23) \end{aligned}$$

with $v_s^2(r) = \partial p(r)/\partial \epsilon(r)$ (squared sound velocity) ([Hinderer et al. 2010](#); [Postnikov et al. 2010](#); [Hinderer 2008](#); [Damour & Nagar 2010](#); [Binnington & Poisson 2009](#)).

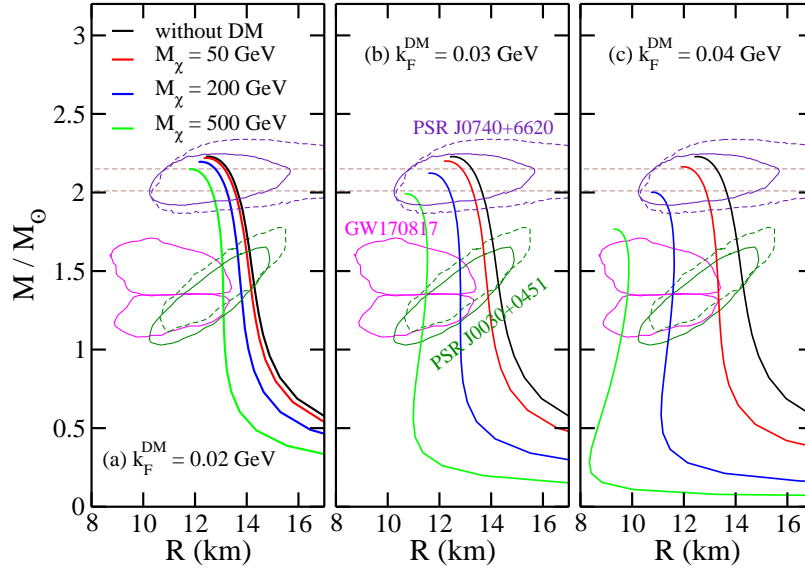


Figure 1. Mass-radius diagrams constructed from the RMF-SRC-DM model for different values of M_χ and k_F^{DM} . Black curves indicate the case in which no DM is included. The contours are related to data from the NICER mission, namely, PSR J0030+0451 (Miller et al. 2019; Riley et al. 2019) and PSR J0740+6620 (Miller et al. 2021; Riley et al. 2021), and the GW170817 event (Abbott et al. 2017, 2018), all of them at 90% credible level. The horizontal lines refer to recent observational constraints on neutron star mass (Fonseca et al. 2021).

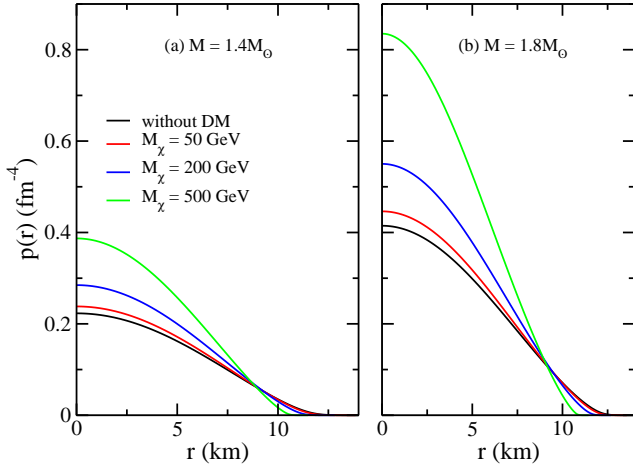


Figure 2. Pressure as a function of the radius for a (a) $1.4M_\odot$, and (b) $1.8M_\odot$ star constructed by taking $k_F^{\text{DM}} = 0.03$ GeV and different values of M_χ . Black curves: case in which no DM is included.

In Fig. 3 we show how Λ depends on the neutron star mass for different RMF-SRC-DM parametrizations. From this figure, it is clear that the increase of M_χ or k_F^{DM} favors the model to reach the limit of $\Lambda_{1,4} = 190^{+390}_{-120}$ provided by LVC (Abbott et al. 2018). In particular, the effect of the M_χ variation is stronger for higher values of the dark particle Fermi momentum, as also verified in the mass-radius diagrams. In Fig. 4 are displayed the tidal deformabilities Λ_1 and Λ_2 of the binary neutron star system (masses M_1 and M_2) associated to the GW170817 event, with $1.37 \leq M_1/M_\odot \leq 1.60$ Abbott et al. (2017). The mass M_2 of the companion star is determined through the relationship between M_1 , M_2 and M (chirp mass) given by (Abbott et al. 2017)

$$\mathcal{M} = (M_1 M_2)^{3/5} / (M_1 + M_2)^{1/5} = 1.188 M_\odot, \quad (24)$$

resulting in $1.17 \leq M_2/M_\odot \leq 1.36$ (Abbott et al. 2017, 2018). The

upper and lower orange lines correspond to the 90% and 50% confidence limits also related to the GW170817 event and provided by LVC (Abbott et al. 2018). From the figure, it is verified that M_χ and k_F^{DM} induce the curves to reach the regions defined by the observational constraint given by the LVC. Notice that the “move” of the curves in direction to the 50% region is more pronounced for the case in which M_χ increases for higher values of k_F^{DM} , exactly as in the case of the observation data for $\Lambda_{1,4}$ in Fig. 3.

3.2 Crustal properties

In this section, we show results provided by the RMF-SRC-DM model concerning the properties related to the neutron star crust (Chamel & Haensel 2008; Haensel et al. 2007; Pethick & Ravenhall 1995; Parmar et al. 2022; Carreau et al. 2019; Lim et al. 2019). The outer layer of this astrophysical compact object, with subsaturation densities, contains only a small fraction of the entire system, typically a few percent of the CS mass. However, the crust physics is very important for the description of the CS phenomenology, namely, cooling, r-processes, oscillations in gamma-ray repeaters, and thermal relaxation in x-ray transients, for instance. In particular, this specific region of a CS needs to be modeled in order to correctly compute the coexistence of an electron gas, a lattice of neutron-rich nuclei, and nonspherical shape structures, such as rods, slabs, waffles, and parking garages (Schneider et al. 2018; Newton & Stone 2009; Schuettrumpf et al. 2019; Avancini et al. 2008), appearing in the so called pasta phase (Ravenhall et al. 1983), namely, a frustrated system in which an intense competition between electromagnetic and strong interactions takes place. For this purpose, some treatments are used to describe the CS crust, such as the piecewise approach used to generate the results presented in the last section, in which the crust is divided into outer and inner parts. Another formulation takes into account an unified equation of state used as input to the TOV equations. In this case, the same hadronic parametrization is applied for the description of all CS regions including the crust

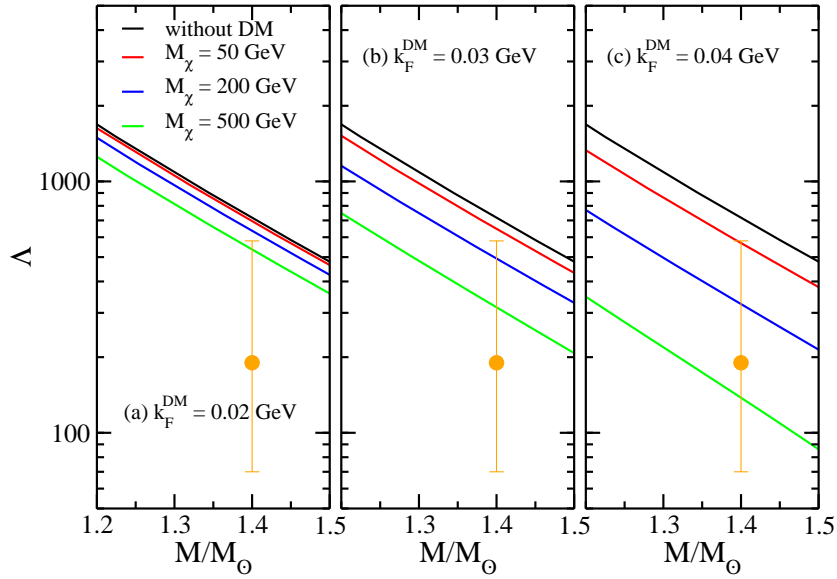


Figure 3. Λ (log scale) as a function of M (solar mass units) constructed from the RMF-SRC-DM model for different values of M_χ and k_F^{DM} . Circle with error bars: result of $\Lambda_{1,4} = 190^{+390}_{-120}$ determined by LVC (Abbott et al. 2018).

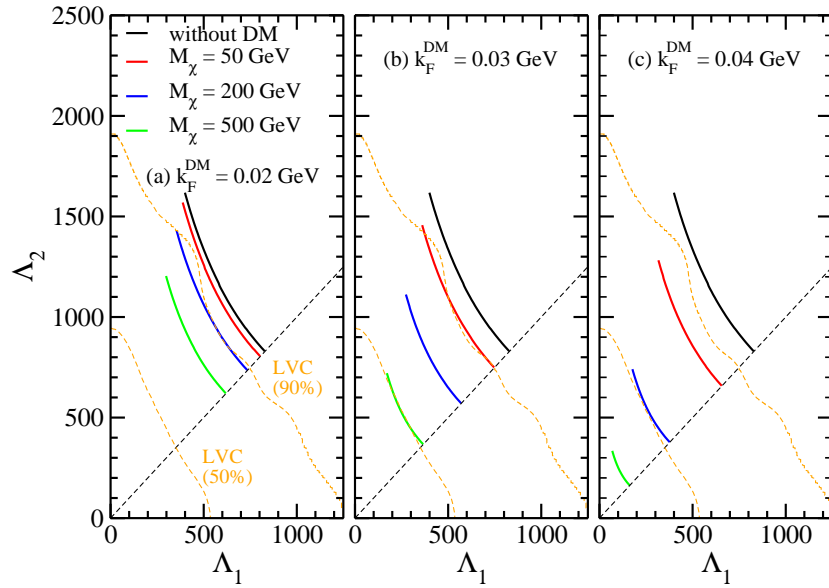


Figure 4. Dimensionless tidal deformabilities for the case of high-mass (Λ_1) and low-mass (Λ_2) components of the GW170817 event. Results obtained from the RMF-SRC-DM model for different values of M_χ and k_F^{DM} . Confidence lines, namely, 90% and 50%, taken from (Abbott et al. 2018).

(outer + inner parts). However, this treatment is more difficult to be implemented. Its construction for different kinds of hadronic models is a hard task, see for instance Mondal et al. (2020) for a study in this direction performed from nonrelativistic Gogny interactions.

Due to the crust structure, namely, a very thin system at low density regime, it is often in the literature the use of suitable approximations capable of providing analytical expressions for some quantities related to this part of the CS (Link et al. 1999; Lattimer & Prakash 2007, 2001; Lorenz et al. 1993). In particular, the studies performed in Fattoyev & Piekarewicz (2010); Piekarewicz et al. (2014) by using $M(r) \approx M$, $p(r) \ll \epsilon(r)$, and $4\pi r^3 p(r) \ll M$, assumed valid in

the crust region, gave rise to

$$M_{\text{crust}}(M) \approx 8\pi R_t^3 p_t \left(\frac{R_t}{2M} - 1 \right) \left[1 + \frac{32p_t}{5\epsilon_t} \left(\frac{R_t}{2M} - \frac{3}{4} \right) \right] \quad (25)$$

for the mass of the CS crust, where R_t , p_t , and ϵ_t are, respectively, radius, pressure, and energy density at the crust-core interface, found in this work as described in the last section, i.e., from the thermodynamical method. This expression is used to generate Fig. 5. Notice that the inclusion of DM content clearly induces a decrease in M_{crust} in both situations: increase of both, k_F^{DM} and M_χ . Once again, more pronounced changes are verified by varying M_χ at higher values of k_F^{DM} .

Fig. 6 depicts how the crustal thickness changes as a function of M for different RMF-SRC-DM parametrizations. In order to determine

this quantity, we proceed by taking $R_{\text{crust}} = R - R_t$. In this calculation, and also in Eq. 25, we obtain R by solving the TOV equations as described in the last section and calculate R_t by associating it to the transition point. Notice that the global behavior verified in the previous results is repeated for R_{crust} . The features displayed in Figs. 5 and 6 indicate that, for a fixed value of M , the increase of dark matter reduces the crustal region since both, mass and thickness, decrease as k_F^{DM} or M_χ increases. Actually, such a reduction also happens for the entire star as one can observe in Fig. 1. For instance, a CS with $M = 1.5M_\odot$ and $k_F^{\text{DM}} = 0.04$ GeV (Fig. 1c) undergoes a reduction in its radius from 13.3 km to 9.9 km as the dark particle mass increases from 50 GeV to 500 GeV. Concerning the crustal region, the same variation in M_χ leads to a change from 1.7 km to 0.50 km in the thickness, and the mass decreases from $4.3 \times 10^{-2}M_\odot$ to $1.5 \times 10^{-2}M_\odot$.

Another important phenomenon that can be explained through properties related to the CS crust is the suddenly spin-up in the rotational frequency of pulsars (Link et al. 1999; Ho et al. 2015), namely, objects that in principle exhibit a very stable rotation, with period from milliseconds to seconds (Hessels et al. 2006). Despite present almost atomic clocks precision, the timing behavior of these particular neutron stars can be modified by jumps in their frequencies. These particular interruptions are called glitches (Lyne 1996; Kaspi et al. 2000), explained from the superfluid vortices exhibited in the neutron star crust (Anderson & Itoh 1975; Pines & Alpar 1985). The difference between the frequencies of the vortices and the entire CS can become high enough so the vortices start a move in the outward direction. In order to preserve the conservation of angular momentum, the rotation of the star is increased giving rise to the glitch. It is possible to associate the glitching mechanism to the crustal fraction of the moment of inertia, I_{crust}/I (Atta et al. 2017; Madhuri et al. 2017; Margaritis et al. 2021). It was shown in Link et al. (1999) that glitches can be explained if $I_{\text{crust}}/I > 1.4\%$, namely, value obtained from the analysis of some known glitching pulsars, such as the Vela one. Furthermore, if crustal entrainment effects are also included in the analysis, this constraint changes to $I_{\text{crust}}/I > 7\%$ (Andersson et al. 2012; Chamel 2013). In order to the capability of the RMF-SRC-DM model to attain this number, we use here the following analytical expression for the crustal moment of inertia,

$$I_{\text{crust}}(M) \approx \frac{16\pi R_t^6 p_t}{6M} \left[1 - \frac{0.21}{(R/2M - 1)} \right] \left[1 + \frac{48p_t}{5\epsilon_t} \left(\frac{R_t}{2M} - 1 \right) \right] \quad (26)$$

also extracted from Fattoyev & Piekarewicz (2010); Piekarewicz et al. (2014). The total moment of inertia is obtained from the solution of the Hartle's slow rotation equation, given by (Landry & Kumar 2018; Hartle 1967; Yagi & Yunes 2013),

$$0 = [r - 2m(r)] \frac{d^2\omega}{dr^2} - 16\pi r [\epsilon(r) + p(r)] \omega(r) + 4 \left\{ \left(1 - \frac{2m(r)}{r} \right) - \pi r^2 [\epsilon(r) + p(r)] \right\} \frac{d\omega}{dr}, \quad (27)$$

and coupled to the TOV equations. From the function $\omega(r)$, one determines $I = R^3(1 - \omega_R)/2$, in which $\omega_R \equiv \omega(R)$.

In Fig. 7 it is depicted the quantity I_{crust}/I , for the model with dark matter included, alongside the aforementioned observational constraint of 7% for this quantity.

As one can see, the increase of dark matter content, by increasing the dark Fermi momentum, causes the decrease in the crustal fraction of the moment of inertia for all ranges of CS mass investigated. This effect is compatible with the reduction of the crust region previously

discussed. The variation in M_χ also produces the same effect, in this case, more significant for higher values of k_F^{DM} , a feature observed in all results presented before. It is worth to mention that the effect in I_{crust}/I observed by the inclusion of DM is due to the variation in both, the total moment of inertia (I) and the moment of inertia of the crust (I_{crust}) itself. Both quantities are affected by variations in k_F^{DM} and M_χ . Furthermore, it is clear that even DM producing reduction in I_{crust}/I , it is still possible to find parametrizations of the RMF-SRC-DM model in agreement with $I_{\text{crust}}/I > 7\%$, i.e., the presence of dark matter can be a possible explanation to the glitch activity in rotation-powered pulsars with exhibiting entrainment effects. In order to verify more clearly this situation, we present in Fig. 8 the crustal fraction of the moment of inertia for a canonical $1.4M_\odot$ CS. The value $M = 1.4M_\odot$ was adopted for the Vela pulsar in Pavlov et al. (2001) to fit its x-ray spectrum. However, it is worth remarking that this is an estimation and not a real measurement of the Vela mass (not precisely known). Other estimations are found in literature, for instance in Ho et al. (2015) in which the value $M = (1.51 \pm 0.04)M_\odot$ was used. From the figure it is verified that all parametrizations are compatible with $I_{\text{crust}}/I > 1.4\%$ regardless the value of M_χ or k_F^{DM} , i.e., there is always some DM content capable of describing the glitching mechanism with no entrainment effects for a pulsar of $1.4M_\odot$. If the constraint analyzed is the $I_{\text{crust}}/I > 7\%$ one, then it is still possible to construct a parametrization with $50 \text{ GeV} \leq M_\chi \leq 500 \text{ GeV}$, however, higher values of M_χ must be followed by lower values of k_F^{DM} in order to satisfy the condition.

4 SUMMARY AND CONCLUDING REMARKS

In this work, we extended the studies performed in Lourenço et al. (2022a,b), in which a nucleonic short-range correlated relativistic hadronic model coupled with dark matter was used to describe neutron star properties. Here we used the same structure of the refereed RMF-SRC-DM model and allowed the variation of the dark particle in the range of $50 \text{ GeV} \leq M_\chi \leq 500 \text{ GeV}$, in agreement with data of spin-independent scattering cross-sections obtained from PandaX-II (Tan et al. 2016), LUX (Akerib et al. 2017), and DarkSide (Marini et al. 2016) collaborations.

We have shown that it is possible to find parametrizations with dark matter content capable of simultaneously attaining observational data, in the mass-radius diagram, regarding NASA's Neutron star Interior Composition Explorer (NICER) mission, the GW170817 event detected by the LIGO and Virgo collaboration (LVC), and recent data on the neutron star mass provided by Fonseca et al. (2021). Our findings also pointed out the feature that the increase of M_χ favors the model to attain the data of $\Lambda_{1.4} = 190_{-120}^{+390}$ determined by LVC (Abbott et al. 2018), and the ones in the $\Lambda_1 \times \Lambda_2$ region related to the neutron stars of the binary system.

Furthermore, we also calculated some crustal properties, namely, mass (M_{crust}), thickness (R_{crust}) and crustal fraction of the moment of inertia (I_{crust}/I). We verified that the increase of M_χ also produces a reduction of the neutron star crust, i.e., M_{crust} and R_{crust} decrease in this situation. Concerning I_{crust}/I , it was shown that this quantity decreases as a function of both, M_χ and the Fermi momentum of the dark particle. However, we verified that it is possible to find RMF-SRC-DM parametrizations that satisfy the constraints $I_{\text{crust}}/I > 1.4\%$ and $I_{\text{crust}}/I > 7\%$, both related to the glitching mechanism of rotation-powered pulsars, such as the Vela one. The latter is obtained when entrainment effects are taken into account in the glitch activity. As a direct consequence, we verified that dark matter can also be used to help describe the glitch phenomenon in pulsars.

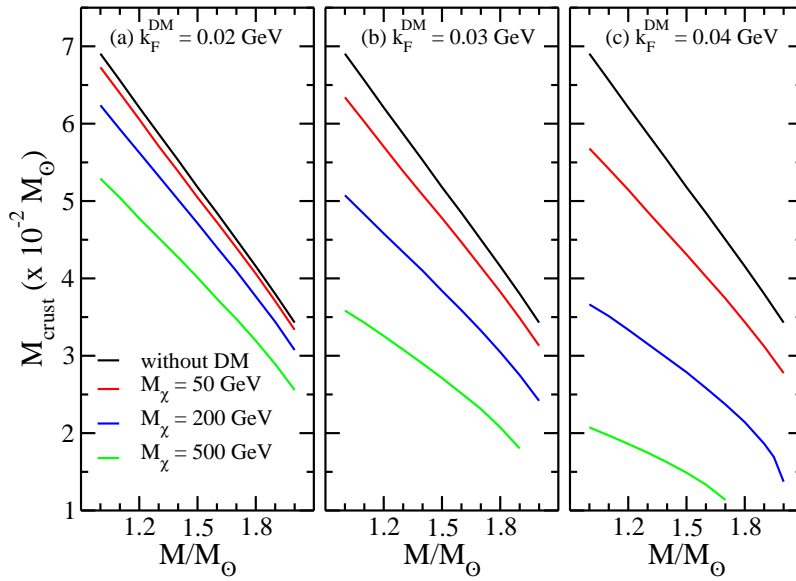


Figure 5. Neutron star crustal mass against the total mass M (solar mass units), constructed from the RMF-SRC-DM model for different values of M_χ and k_F^{DM} . Black curves indicate the case in which no DM is included.

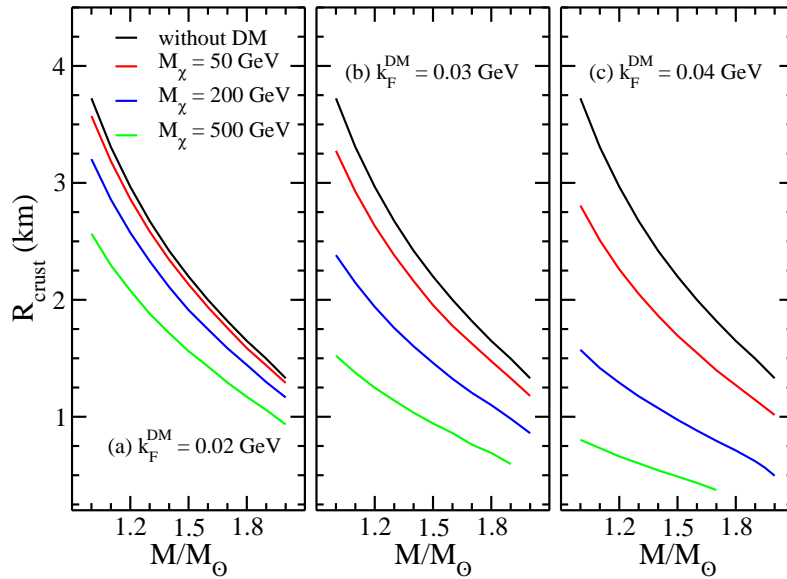


Figure 6. Neutron star crustal thickness against the total mass M (solar mass units), constructed from the RMF-SRC-DM model for different values of M_χ and k_F^{DM} . Black curves indicate the case in which no DM is included.

ACKNOWLEDGMENTS

This work is a part of the project INCT-FNA proc. No. 464898/2014-5. It is also supported by Conselho Nacional de Desenvolvimento Científico e Tecnológico (CNPq) under Grants No. 312410/2020-4 (O.L.), and No. 308528/2021-2 (M.D.). We also acknowledge Fundação de Amparo à Pesquisa do Estado de São Paulo (FAPESP) under Thematic Project 2017/05660-0 and Grant No. 2020/05238-9.

DATA AVAILABILITY STATEMENT

This manuscript has no associated data or the data will not be deposited. All data generated during this study are contained in this published article.

REFERENCES

- Abbott B. P., et al., 2016a, *Phys. Rev. X*, 6, 041015
- Abbott B. P., et al., 2016b, *Phys. Rev. Lett.*, 116, 061102
- Abbott B. P., et al., 2016c, *Phys. Rev. Lett.*, 116, 241103
- Abbott B. P., et al., 2017, *Phys. Rev. Lett.*, 119, 161101
- Abbott B. P., et al., 2018, *Phys. Rev. Lett.*, 121, 161101
- Abbott B. P., et al., 2020, *The Astrophysical Journal Letters*, 892, L3

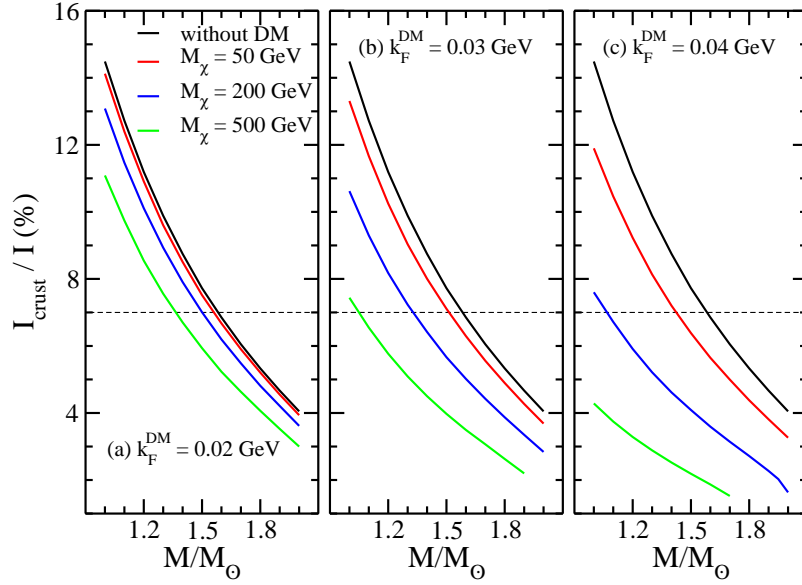


Figure 7. Crustal fraction of the moment of inertia as a function of stellar mass for M (solar mass units), constructed from the RMF-SRC-DM model for different values of M_χ and k_F^{DM} . The horizontal lines indicate the constraint of 7%.

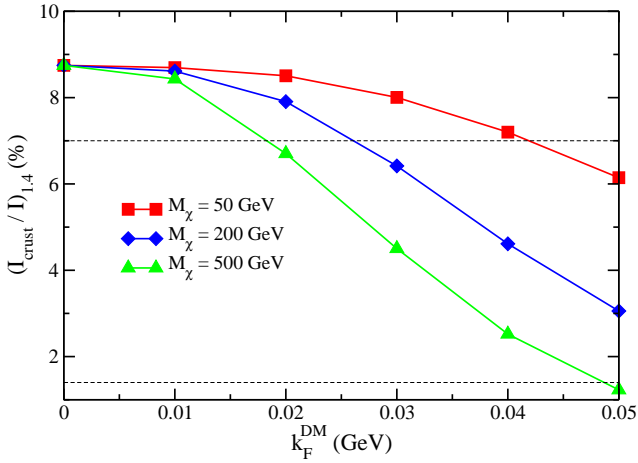


Figure 8. I_{crust}/I for a canonical CS of $1.4M_\odot$ as a function of the Fermi dark moment, obtained from the RMF-SRC-DM model for different values of M_χ . The horizontal lines indicate the constraints of 1.4% and 7%.

Adhikari D., et al., 2021, *Phys. Rev. Lett.*, 126, 172502
 Akerib D. S., et al., 2017, *Phys. Rev. Lett.*, 118, 021303
 Anderson P. W., Itoh N., 1975, *Nature*, 256, 25
 Andersson N., Glampedakis K., Ho W. C. G., Espinoza C. M., 2012, *Phys. Rev. Lett.*, 109, 241103
 Annala E., Gorda T., Kurkela A., Nättilä J., Vuorinen A., 2020, *Nature Physics*, 16, 907
 Atta D., Mukhopadhyay S., Basu D. N., 2017, *Indian Journal of Physics*, 91, 235
 Avancini S. S., Menezes D. P., Alloy M. D., Marinelli J. R., Moraes M. M. W., Providência C., 2008, *Phys. Rev. C*, 78, 015802
 Baym G., Pethick C., Sutherland P., 1971, *ApJ*, 170, 299
 Bhat S. A., Paul A., 2020, *European Physical Journal C*, 80, 544
 Binnington T., Poisson E., 2009, *Phys. Rev. D*, 80, 084018
 CLAS Collaboration 2018, *Nature*, 560, 617
 CLAS Collaboration 2019, *Nature*, 566, 354
 Cai B.-J., Li B.-A., 2016, *Phys. Rev. C*, 93, 014619
 Cai B.-J., Li B.-A., 2022, *Phys. Rev. C*, 105, 064607

Carreau T., Gulminelli F., Margueron J., 2019, *Phys. Rev. C*, 100, 055803
 Carriere J., Horowitz C. J., Piekarewicz J., 2003, *The Astrophysical Journal*, 593, 463
 Chamel N., 2013, *Phys. Rev. Lett.*, 110, 011101
 Chamel N., Haensel P., 2008, *Living Reviews in Relativity*, 11, 10
 Cline J. M., Scott P., Kainulainen K., Weniger C., 2013, *Phys. Rev. D*, 88, 055025
 Cline J. M., Kainulainen K., Scott P., Weniger C., 2015, *Phys. Rev. D*, 92, 039906
 Cowperthwaite P. S., et al., 2017, *ApJ*, 848, L17
 Damour T., Nagar A., 2010, *Phys. Rev. D*, 81, 084016
 Das A., Malik T., Nayak A. C., 2019, *Phys. Rev. D*, 99, 043016
 Das H. C., Kumar A., Kumar B., Biswal S. K., Nakatsukasa T., Li A., Patra S. K., 2020, *Monthly Notices of the Royal Astronomical Society*, 495, 4893
 Das H. C., Kumar A., Patra S. K., 2021a, *Phys. Rev. D*, 104, 063028
 Das H. C., Kumar A., Biswal S. K., Patra S. K., 2021b, *Phys. Rev. D*, 104, 123006
 Das H. C., Kumar A., Patra S. K., 2021c, *Monthly Notices of the Royal Astronomical Society*, 507, 4053
 Das H., Kumar A., Kumar B., Biswal S., Patra S., 2021d, *Journal of Cosmology and Astroparticle Physics*, 2021, 007
 Das H. C., Kumar A., Kumar B., Patra S. K., 2022a, *Galaxies*, 10
 Das A., Malik T., Nayak A. C., 2022b, *Phys. Rev. D*, 105, 123034
 Duer M., et al., 2019, *Physics Letters B*, 797, 134792
 Dutra M., Lourenço O., Sá Martins J. S., Delfino A., Stone J. R., Stevenson P. D., 2012, *Phys. Rev. C*, 85, 035201
 Dutra M., et al., 2014a, *Phys. Rev. C*, 90, 055203
 Dutra M., et al., 2014b, *Phys. Rev. C*, 90, 055203
 Dutra M., Lourenço O., Menezes D. P., 2016a, *Phys. Rev. C*, 93, 025806
 Dutra M., Lourenço O., Menezes D. P., 2016b, *Phys. Rev. C*, 94, 049901
 Este J., et al., 2021, *Phys. Rev. Lett.*, 126, 162701
 Fattoyev F. J., Piekarewicz J., 2010, *Phys. Rev. C*, 82, 025810
 Feng J. L., 2010, *Annual Review of Astronomy and Astrophysics*, 48, 495
 Fonseca E., et al., 2021, *The Astrophysical Journal Letters*, 915, L12
 Frederico T., Carlson B. V., Rego R. A., Hussein M. S., 1989, *Journal of Physics G: Nuclear and Particle Physics*, 15, 297
 Gendreau K. C., et al., 2016, in den Herder J.-W. A., Takahashi T., Bautz M., eds, Vol. 9905, *Space Telescopes and Instrumentation 2016: Ultraviolet to Gamma Ray*. SPIE, p. 99051H, doi:10.1117/12.2231304, <https://doi.org/10.1117/12.2231304>

- Giangrandi E., Sagun V., Ivanytskyi O., Providência C., Dietrich T., 2022, The effects of self-interacting bosonic dark matter on neutron star properties, [doi:10.48550/ARXIV.2209.10905](https://arxiv.org/abs/2209.10905), <https://arxiv.org/abs/2209.10905>
- Gonzalez-Boquera C., Centelles M., Viñas X., Robledo L., 2018, *Physics Letters B*, 779, 195
- Gonzalez-Boquera C., Centelles M., Viñas X., Routray T. R., 2019, *Phys. Rev. C*, 100, 015806
- Guha A., Sen D., 2021, *Journal of Cosmology and Astroparticle Physics*, 2021, 027
- Guichon P. A. M., 1988, *Physics Letters B*, 200, 235
- Guichon P. A. M., Stone J. R., Thomas A. W., 2018, *Progress in Particle and Nuclear Physics*, 100, 262
- Guo W.-M., Li B.-A., Yong G.-C., 2021, *Phys. Rev. C*, 104, 034603
- Haensel P., Potekhin A. Y., Yakovlev D. G., 2007, *Neutron stars 1: Equation of state and structure*. Vol. 326, Springer, New York, USA, [doi:10.1007/978-0-387-47301-7](https://doi.org/10.1007/978-0-387-47301-7)
- Hartle J. B., 1967, *ApJ*, 150, 1005
- Hen O., et al., 2014, *Science*, 346, 614
- Hen O., Miller G. A., Piasetzky E., Weinstein L. B., 2017, *Rev. Mod. Phys.*, 89, 045002
- Hessels J. W. T., Ransom S. M., Stairs I. H., Freire P. C. C., Kaspi V. M., Camilo F., 2006, *Science*, 311, 1901
- Hinderer T., 2008, *The Astrophysical Journal*, 677, 1216
- Hinderer T., Lackey B. D., Lang R. N., Read J. S., 2010, *Phys. Rev. D*, 81, 123016
- Ho W. C. G., Espinoza C. M., Antonopoulou D., Andersson N., 2015, *Science Advances*, 1, e1500578
- Kaspi V. M., Lackey J. R., Chakrabarty D., 2000, *ApJ*, 537, L31
- Kubis S., 2004, *Phys. Rev. C*, 70, 065804
- Kumar A., Das H. C., Patra S. K., 2022, *Monthly Notices of the Royal Astronomical Society*, 513, 1820
- Kusenko A., Rosenberg L. J., 2013, Snowmass-2013 Cosmic Frontier 3 (CF3) Working Group Summary: Non-WIMP dark matter, [doi:10.48550/ARXIV.1310.8642](https://arxiv.org/abs/1310.8642), <https://arxiv.org/abs/1310.8642>
- Landry P., Kumar B., 2018, *ApJ*, 868, L22
- Lattimer J. M., 2012, *Annual Review of Nuclear and Particle Science*, 62, 485
- Lattimer J. M., Prakash M., 2001, *The Astrophysical Journal*, 550, 426
- Lattimer J. M., Prakash M., 2007, *Physics Reports*, 442, 109
- Li B.-A., Chen L.-W., Ko C. M., 2008, *Phys. Rep.*, 464, 113
- Lim Y., Holt J. W., Stahulak R. J., 2019, *Phys. Rev. C*, 100, 035802
- Link B., Epstein R. I., Lattimer J. M., 1999, *Phys. Rev. Lett.*, 83, 3362
- Lorenz C. P., Ravenhall D. G., Pethick C. J., 1993, *Phys. Rev. Lett.*, 70, 379
- Lourenço O., Dutra M., Lenzi C. H., Biswal S. K., Bhuyan M., Menezes D. P., 2020, *European Physical Journal A*, 56, 32
- Lourenço O., et al., 2021, *Chinese Physics C*, 45, 025101
- Lourenço O., Frederico T., Dutra M., 2022a, *Phys. Rev. D*, 105, 023008
- Lourenço O., Lenzi C. H., Frederico T., Dutra M., 2022b, *Phys. Rev. D*, 106, 043010
- Lyne A. G., 1996, *International Astronomical Union Colloquium*, 160, 73
- Madhuri K., Basu D. N., Routray T. R., Pattnaik S. P., 2017, *European Physical Journal A*, 53, 151
- Malik T., Agrawal B. K., De J. N., Samaddar S. K., Providência C., Mondal C., Jha T. K., 2019, *Phys. Rev. C*, 99, 052801
- Margaritis C., Koliogiannis P. S., Kanakis-Pegios A., Moustakidis C. C., 2021, *Phys. Rev. C*, 104, 025805
- Marini L., et al., 2016, *Nuovo Cimento C Geophysics Space Physics C*, 39, 247
- Menezes D. P., 2021, *Universe*, 7
- Miller M. C., et al., 2019, *The Astrophysical Journal*, 887, L24
- Miller M. C., et al., 2021, *The Astrophysical Journal Letters*, 918, L28
- Mondal C., Viñas X., Centelles M., De J. N., 2020, *Phys. Rev. C*, 102, 015802
- Newton W. G., Stone J. R., 2009, *Phys. Rev. C*, 79, 055801
- Oort J. H., 1932, *Bull. Astron. Inst. Netherlands*, 6, 249
- Oppenheimer J. R., Volkoff G. M., 1939, *Phys. Rev.*, 55, 374
- Panotopoulos G., Lopes I., 2017, *Phys. Rev. D*, 96, 083004
- Parmar V., Das H. C., Kumar A., Sharma M. K., Patra S. K., 2022, *Phys. Rev. D*, 105, 043017
- Pavlov G. G., Zavlin V. E., Sanwal D., Burwitz V., Garmire G. P., 2001, *ApJ*, 552, L129
- Pethick C. J., Ravenhall D. G., 1995, *Annual Review of Nuclear and Particle Science*, 45, 429
- Piekarewicz J., Fattoyev F. J., 2019, *Phys. Rev. C*, 99, 045802
- Piekarewicz J., Fattoyev F. J., Horowitz C. J., 2014, *Phys. Rev. C*, 90, 015803
- Pines D., Alpar M. A., 1985, *Nature*, 316, 27
- Postnikov S., Prakash M., Lattimer J. M., 2010, *Phys. Rev. D*, 82, 024016
- Quddus A., Panotopoulos G., Kumar B., Ahmad S., Patra S. K., 2020, *Journal of Physics G: Nuclear and Particle Physics*, 47, 095202
- Ravenhall D. G., Pethick C. J., Wilson J. R., 1983, *Phys. Rev. Lett.*, 50, 2066
- Reed B. T., Fattoyev F. J., Horowitz C. J., Piekarewicz J., 2021, *Phys. Rev. Lett.*, 126, 172503
- Riley T. E., et al., 2019, *The Astrophysical Journal*, 887, L21
- Riley T. E., et al., 2021, *The Astrophysical Journal Letters*, 918, L27
- Rubin V. C., Ford W. K. J., Thonnard N., 1978, *ApJ*, 225, L107
- Sagun V., et al., 2022, *PoS, PANIC2021*, 313
- Schmidt A., et al., 2020, *Nature*, 578, 540
- Schneider A. S., Caplan M. E., Berry D. K., Horowitz C. J., 2018, *Phys. Rev. C*, 98, 055801
- Schuetrumpf B., Martínez-Pinedo G., Afibuzzaman M., Aktulga H. M., 2019, *Phys. Rev. C*, 100, 045806
- Sen D., Guha A., 2021, *Monthly Notices of the Royal Astronomical Society*, 504, 3354
- Souza L. A., Dutra M., Lenzi C. H., Lourenço O., 2020, *Phys. Rev. C*, 101, 065202
- Stone J. R., 2021, *Universe*, 7
- Stone J. R., Guichon P. A. M., Thomas A. W., 2022, *Frontiers in Astronomy and Space Sciences*, 9
- Tan A., et al., 2016, *Phys. Rev. Lett.*, 117, 121303
- Tolman R. C., 1939, *Phys. Rev.*, 55, 364
- Xu J., Chen L.-W., Li B.-A., Ma H.-R., 2009, *The Astrophysical Journal*, 697, 1549
- Yagi K., Yunes N., 2013, *Phys. Rev. D*, 88, 023009
- Zwicky F., 1933, *Helvetica Physica Acta*, 6, 110
- Zwicky F., 2009, *General Relativity and Gravitation*, 41, 207